IET Microwaves, Antennas & Propagation

Research Article

Dual-wideband filter with wide high-rejection band using composite resonators

ISSN 1751-8725
Received on 19th April 2018
Revised 20th November 2018
Accepted on 14th December 2018
E-First on 25th January 2019
doi: 10.1049/iet-map.2018.5177
www.ietdl.org

Zhiliang Li[1], Ke-Li Wu[1] ✉

[1]Department of Electronic Engineering, The Chinese University of Hong Kong, Shatin, NT, Hong Kong, People's Republic of China

✉ *E-mail: klwu@ee.cuhk.edu.hk*

Abstract: A new type of dual-wideband bandpass filter using composite series and shunt resonators is proposed in conjunction with its direct synthesis and design theory. By making use of the transmission pole (TP) and the transmission zero of the composite resonators flexibly, a dual-wideband filter with a wide range of frequency and bandwidth ratios as well as a wide stopband can be realised. With a shunt capacitor introduced at each I/O port, extra TPs either in the low passband or in the high passband can be created, leading to more filter design options. To give a direct design procedure, a lumped-element prototype is first synthesised based on a target filtering function and a dedicated circuit extraction process. The filter layout can be realised using semi-distributed circuits and chip capacitors. Two practical schemes are introduced to suppress spurious resonances for a wide high-rejection stopband. Two filter examples are designed with a small and a large frequency ratio and a wide band suppressed spurious resonances. The unique filter response and good agreement between the designed and measured results demonstrate the superior performance of the proposed filter structure and the effectiveness of the synthesis and design theory.

1 Introduction

Due to the high demands on co-existence of multiple wireless services in different frequency bands over the same wireless infrastructure, it is desirable to combine multiple services that operate at different frequencies into a shared device, such as a wideband or dual wideband antenna. To meet this requirement, dual-band bandpass filters (BPFs) are needed in the component chain. Until now, there have been many research efforts in developing dual-band BPFs. In a straight-forward way, dual-band BPFs can be built by two parallel-connected single-band BPFs [1] or a wideband BPF cascaded by a bandstop filter [2]. Since stepped-impedance resonators (SIRs) provide a flexible control of the frequency ratio of the fundamental and the first higher order mode, they have been widely used in constructing dual-band BPFs [3, 4]. Dual-mode resonators have also been used to design dual-band BPFs in [5]. Another popular approach to realise a dual-band BPF is to design a high-order filter with inserted transmission zeros (TZs) between two passbands [6, 7]. This approach has been widely applied to the design of dual-narrowband filters, which can be modelled and synthesised by coupled resonator networks. However, the traditional coupled resonator network is not applicable to a wide passband dual-band filter as it could not reflect the dispersion effects of the resonators and the coupling structures in a wide frequency range. Though some dual-wideband filter structures have been proposed, most of these filters are designed by intuitive tuning and optimisation except a few of recent works [8–10], in which a commensurate-line network is used to achieve a dual-wideband operation. By following a direct synthesis approach, the circuit parameters can be directly determined from specifications. In these works, the two passbands always share the same order, and the flexibility of prescribing TZs is limited by the classical or modified Richard's transformation used. Moreover, the designs suffer from unwanted periodic spurious resonances, which limits the bandwidth of upper stopband.

In the literature of dual-band BPFs, much research emphasis has been placed on the enhancement of skirt selectivity and inter-band isolation. In many practical applications, it is also important for dual-wideband filters to have a wide spurious-free upper stopband. To achieve a sufficient rejection in a wide upper stopband, three methods are commonly used: using SIRs to push up spurious resonances [11]; using dissimilar resonators having the same resonant frequency in the working band but dispersed higher order frequencies; and using TZs to suppress the spurious resonances [12]. In [13, 14], a combination of dissimilar resonators and TZs is used to extend the upper stopband for dual-narrowband BPFs.

In [15], a wide single band filter composed of inductively coupled shunt composite resonators is proposed with a wide high rejection stopband by legitimately placing TZs in the stopband. The concept is extended to a wide single band filter with TZs on the both sides of the passband using both series and shunt composite resonators [16]. In [15, 16], the lumped element filter prototype is systematically approximated by a mixed lumped/distributed (MLD) circuit in a wide frequency range. It is found that the composite resonators are very useful in constructing wideband filters of different responses.

In this work, a dual-wideband BPF configuration that comprises cascaded composite series and shunt resonators and a shunt capacitor at each I/O port, as depicted in Fig. 1, is proposed. The two shunt capacitors at I/O ports provide a legitimate control on I/O couplings as well as contribute two extra TPs within passbands and far TZs to suppress spurious resonances by making use of their parasitic inductors. Taking the advantage that each composite resonator can produce a transmission pole (TP) and a TZ, with which TP is larger than TZ for the composite series resonator but smaller than TZ for the composite shunt resonator, a dual-wideband filter can be constructed with much flexibility. The proposed dual-wideband filter configuration has two different design options depending on which passband the two extra TPs are assigned to. The first design option with the extra TPs being assigned to the low passband is suitable for the applications of a small fractional bandwidth (FBW) ratio of the high passband to the low passband. The other design option with the extra TPs being assigned to the high passband is suitable for the applications of a large FBW ratio of the high passband to the low passband. By appropriately arranging TPs and TZs, a dual-band response with a high skirt selectivity can be achieved. The filtering function that features a Chebyshev-like response can be synthesised by iteratively solving a linear problem. Then the lumped elements of the filter prototype can be determined through a dedicated circuit extraction process.

Unlike the cases for wide single band filters in [15, 16], it is difficult to analytically establish a MLD circuit approximation in

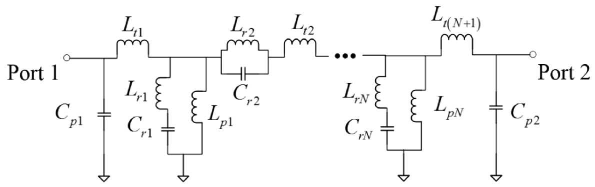

Fig. 1 *Typical circuit topology of the proposed dual-wideband BPF comprising shunt capacitors at I/O ports and composite series and shunt resonators*

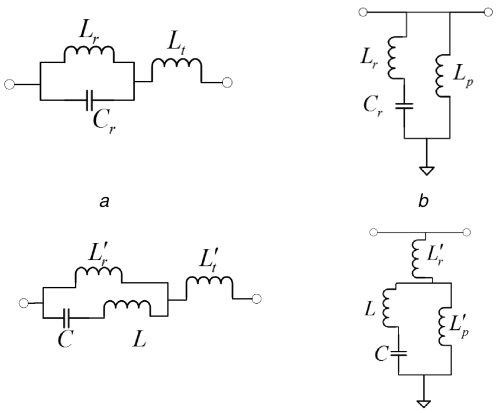

Fig. 2 *Circuit models of composite resonators*
(a) Basic form of composite series resonator, ***(b)*** Basic form of composite shunt resonator, ***(c)*** Equivalent form of composite series resonator, ***(d)*** Equivalent form of composite shunt resonator

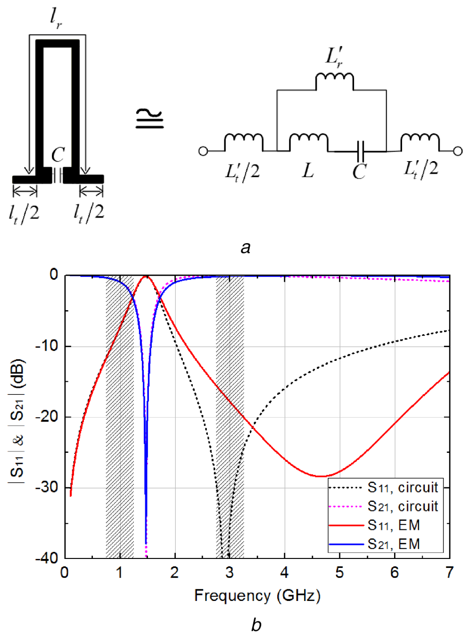

Fig. 3 *Realisation of composite series resonator*
(a) Physical layout of composite series resonator, ***(b)*** Response comparison between the circuit model and EM model of the resonator (the shaded frequency ranges are the low and high passbands)

two wide passbands. To minimise the response deviation of a physical model from the lumped element prototype, high-impedance transmission lines (HITLs) are used to implement the inductors, whereas the capacitors are realised by radial stubs or chip capacitors. Usually, below the frequency of the first spurious resonance of semi-lumped elements, the synthesised *LC* element filter prototype can serve as a good wideband circuit model to help tune the return losses in passbands to be below −15 dB or even better. Nevertheless, cases may happen that the small discrepancy between the lumped element model and the physical layout makes the fine tuning difficult. In such cases, one can use the wideband MLD element model instead for fine tuning. The MLD element model can be generally obtained by optimisation despite being analytically unavailable.

Although the basic features of the dual-wideband filter configuration and its filtering function have been reported in [17], the working principle and the design theory of the dual-wideband filter are not addressed. In this paper, the working principle of the filter and the general synthesis and design theory are presented, providing more insight and a complete design theory of this new type of dual-wideband BPF. In addition to more design options, more importantly, the schemes of suppressing spurious resonances using far TZs are fully discussed through two design examples in this extended work.

2 Composite series and shunt resonators

As shown in Figs. 2*a* and *b*, a composite series resonator consists of an *LC* tank and a series inductor, whereas a composite shunt resonator consists of a series *LC* circuit and a shunt inductor. As proved in [16], the TP frequency is always larger than the TZ frequency for the composite series resonator and smaller than the TZ frequency for the composite shunt resonator. Their equivalent circuits are shown in Figs. 2*c* and *d*, respectively, which are introduced for convenience of layout design. For a composite series resonator, if L is known, its equivalent circuit can be obtained as

$$L'_r = \frac{1}{2}\left(L_r + \sqrt{L_r^2 + 4LL_r}\right) \tag{1}$$

$$L'_t = L_t - \frac{LL'_r}{L + L'_r} \tag{2}$$

$$C = \frac{L_r}{L + L'_r} C_r \tag{3}$$

For a composite shunt resonator, if L is known, its equivalent circuit can be obtained as

$$L'_p = \frac{L_p^2 + \sqrt{L_p^4 + 4LL_p^2(L_p + L_r)}}{2(L_p + L_r)} \tag{4}$$

$$L'_r = L_p - L'_p \tag{5}$$

$$C = \frac{L_p + L_r}{L + L'_p} C_r \tag{6}$$

In the equivalent circuits, C can be implemented by a chip capacitor and L represents the parasitic inductance of the chip capacitor and its connecting terminals.

In [17], the composite resonators were briefly discussed with no design details. Here details are provided about how the composite resonators are dimensioned according to their circuit models. Fig. 3*a* shows a typical microstrip line realisation of a composite series resonator on a Rogers 5880 substrate that is with relative permittivity of 2.2 and thickness of 0.508 mm (the same substrate will be used in the design examples in Section 5). With the element values obtained by the direct synthesis procedure, the equivalent resonator circuit can be obtained using (1)–(3) after estimating the parasitic inductance L. Using one of the composite series resonators in the first design example for illustration here, in which $L'_r = 3.76$ nH, $L'_t = 0.55$ nH, $L = 0.77$ nH, and $C = 2.4$ pF. By choosing the width of HITLs to be 0.23 mm, the line length l_r is estimated to be 8.4 mm by [18]

$$l_r = \frac{\lambda_g}{2\pi}\sin^{-1}\left(\frac{\omega_0 L'_r}{Z_c}\right) \tag{7}$$

where Z_c is the characteristic impedance of HITL, λ_g is the guided wavelength at ω_0 ($\omega_0 = 4\pi \times 10^9$ rad/s), and ω_0 is the angular centre frequency between the two passbands. Similarly, the line length l_t

is estimated as 1.1 mm. Due to the parasitic effects and junction discontinuities, the initial layout of the resonator needs to be fine-tuned with final dimensions $l_r = 10.9$ mm and $l_t = 1.66$ mm. With the full-wave simulator HFSS, the EM response can be obtained and is compared with the circuit model response in Fig. 3*b*. As can be observed, the circuit model can well represent the physical resonator in a wide frequency range covering the two wide passbands centred at 1 and 3 GHz, respectively. Note that the discrepancy in the high passband is small in absolute value.

As shown in Fig. 4*a*, a composite shunt resonator is realised by a grounded stub in parallel with a radial-stub-loaded transmission line. The circuit element values are $L_p = 9.41$ nH, $L_r = 1.43$ nH, and $C_r = 1.44$ pF. With the width of HITLs fixed as 0.23 mm, the line length l_r for realising L_r is estimated to be 2.9 mm using (7) and the length of the short-circuit HITL inductor l_p can be estimated to be 14.6 mm by [18]

$$l_p = \frac{\lambda_g}{2\pi}\tan^{-1}\left(\frac{\omega_0 L_p}{Z_c}\right) \tag{8}$$

As there is no simple design formula for calculating the equivalent capacitance of radial stub, its dimensions can be designed by comparing the response of its EM model and that of the circuit model. The obtained dimensions are $l_r = 2.58$ mm, $l_p = 27.6$ mm, $r = 5.72$ mm, and $\alpha = 1.34$ rad. The final length l_p is quite different from the calculated one using (8) because (8) assumes a straight-line stub but a meander line part is used in implementation here. The responses of the EM model and circuit model are compared in Fig. 4*b*, from which a good agreement can be observed in the two passbands.

Using chip capacitors and quasi-lumped element circuits, both composite series and shunt resonators can be realised in a good accordance with their circuit models over a wide frequency range. Since the layout of each resonator is designed separately, the initial layout of a filter can be assembled by cascading them together. To take into account the parasitic effects and to optimise the spurious performance, the initial layout dimensions have to be further optimised. Nevertheless, the initial layout serves as a good starting point for EM optimisation.

3 Dual-band filter using composite resonators

To construct a dual-wideband filter, the two types of composite resonators can be combined. As discussed in [17], the basic idea behind the dual-band operation is to arrange TPs and TZs into different passbands and stopbands, respectively. Here it seeks to give a full explanation of the working principle in an intuitive way. As shown in Fig. 5*a*, a composite shunt resonator is cascaded to a composite series resonator on the right side, resulting in a basic dual-band filter. As illustrated in Fig. 5*b*, the overall transmission response of the basic dual-band filter is roughly a multiplication of the individual transmission responses of the two composite resonators, which provides an intuitive insight into the working principle of the dual-wideband filter. Before the cascading, the TP and TZ frequencies of the shunt resonator are denoted as f_{p1} and f_{z1}, respectively, and those for the series resonator are denoted by f_{p2} and f_{z2}, respectively. Assume $f_{p1} < f_{z2}$ and $f_{p2} > f_{z1}$, the basic filter block exhibits a dual-band response with all TZs located between the two passbands. The shunt and series resonators contribute to the low and the high resonances, respectively. After the cascading, the two TZs remain unchanged but the two TPs are shifted from f_{p1} to f'_{p1}, and f_{p2} to f'_{p2}, respectively.

To improve the selectivity in the low and high stopbands, TZs can be introduced in these stopbands by cascading more composite resonators to the basic dual-band filter. In Fig. 6*a*, the basic dual-band filter is cascaded with one series resonator on the left side and one shunt resonator on the right side. As can be observed from Fig. 6*b*, the two newly added composite resonators produce two TZs at f_{z3} and f_{z4} in the low and high stopbands, respectively. Meanwhile, the order for each passband of the advanced dual-band filter is increased by one. Overall, the advanced dual-band response exhibits four TPs and four TZs distributed in the three stopbands.

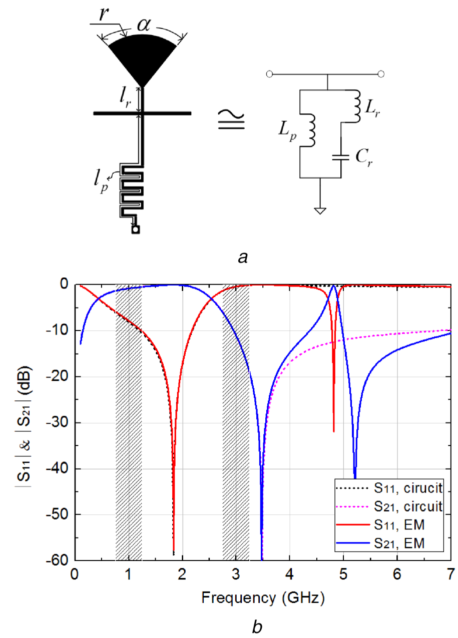

Fig. 4 *Realisation of composite shunt resonator*
(a) Physical layout of composite shunt resonator, ***(b)*** Response comparison between the circuit model and EM model of the resonator (the shaded frequency ranges are the low and high passbands)

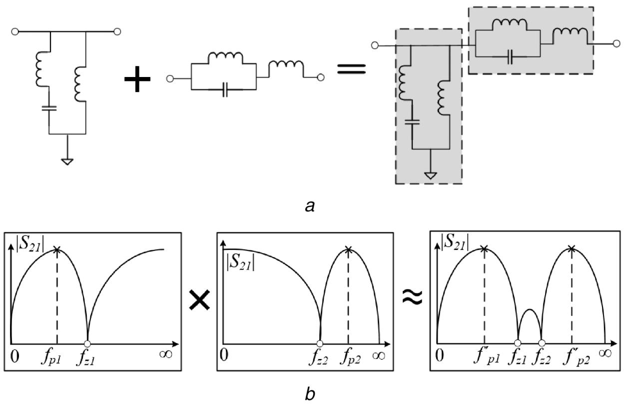

Fig. 5 *Basic dual-band filter prototype*
(a) Circuit configuration as a cascade of composite shunt and series resonators, ***(b)*** Formation of transmission response by multiplication of individual responses of composite resonators

Based on the principle, an arbitrarily-ordered dual-wideband filter can be conveniently constructed. It should be mentioned that the direct cascading usually leads to a poorly matched filter, necessitating additional I/O matching circuits comprising series or shunt inductors, whose element values can be determined from a systematic synthesis process.

Besides the cascaded composite resonators, a shunt capacitor and a series inductor are placed at each I/O port of the proposed dual-wideband filter prototype as shown in Fig. 1. They are introduced not only for providing a legitimate control on I/O couplings, but also generating two extra TPs. Additionally, as the radial stub realising the shunt capacitor possesses parasitic inductors [19], far TZs can be produced at designated frequencies to suppress spurious resonances. Besides making use of parasitic effects of shunt capacitors, it could also introduce far TZs by inserting bandstop blocks of shunt connected series *LC* circuits, as will be discussed in design examples.

4 Synthesis of lumped element filter prototype

For the lumped element circuit shown in Fig. 1, the reflection and transmission coefficients of the filter can be expressed as

$$S_{11} = \frac{F(s)}{E(s)}, \quad S_{21} = \frac{P(s)}{\varepsilon E(s)} \tag{9}$$

where $E(s)$, $F(s)$, and $P(s)$ are real polynomials with the complex frequency variable $s = j\omega$, and ε is the ripple factor. The squared magnitude of the transmission coefficient can also be expressed as

$$|S_{21}|^2 = \frac{1}{1 + (\varepsilon T(s))^2} \tag{10}$$

where $T(s)$ is the filtering function and can be expressed in terms of $F(s)$ and $P(s)$ as

$$T(s) = F(s)/P(s) \tag{11}$$

Assume that the total number of composite series and shunt resonators is N. The circuit configurations that are equivalent to the original circuit at DC and infinity frequency are shown in Fig. 7 [20]. As can be seen, the equivalent circuit has one shunt inductor at DC and three circuit elements including one series inductor and two shunt capacitors at infinity frequency. Therefore, there are one TZ at DC and three TZs at infinity. The N finite TZs are produced by either parallel connected LC series circuits or serially connected LC tanks, and they are all on the imaginary axis of the complex s plane. Since the finite TZs z_i and those at DC are the roots of $P(s)$, the factorised form of $P(s)$ can be expressed as

$$P(s) = p_{2N+1} s \prod_{i=1}^{N} \left(s^2 - s_{zi}^2\right) \tag{12}$$

where $s_{zi} = jz_i$. As there are three TZs at infinity, the degree of $F(s)$ should be three orders higher than that of $P(s)$. The rational expression of the filtering function for the filter circuit configuration in Fig. 1 can be written as

$$T(s) = \frac{s^{2N+4} + f_{2N+3}s^{2N+3} + \cdots + f_1 s^1 + f_0}{p_{2N+1}s^{2N+1} + p_{2N-1}s^{2N-1} + \cdots + p_3 s^3 + p_1 s^1} \tag{13}$$

Since all the circuit LC elements are real valued, the coefficients f_0 through f_{2N+3} and p_1 through p_{2N+1} must be real. Assume all the roots of $F(s)$ are located on the imaginary axis of the s plane, $F(s)$ must be an even polynomial so that (13) can be simplified to

$$T(s) = \frac{s^{2N+4} + f_{2N+2}s^{2N+2} + \cdots + f_2 s^2 + f_0}{p_{2N+1}s^{2N+1} + p_{2N-1}s^{2N-1} + \cdots + p_3 s^3 + p_1 s^1} \tag{14}$$

where $N + 3$ coefficients are to be determined. Define the two passbands as $[\omega_1, \omega_2]$ and $[\omega_3, \omega_4]$, which are of degrees N_1 and N_2, respectively. To achieve an equiripple dual-band response, the ideal $T(j\omega)$ should have a magnitude response as shown in Fig. 8. For each passband, $|T(j\omega)|$ has the same value at two band edges and a number of interior frequency points where $|T(j\omega)|$ reaches the local maximum. As a result, there are $N_1 + N_2 + 2$ constraints in total for an equiripple dual-band response as described by

$$T(j\omega_i) = \begin{cases} \pm j\Delta_1, & \omega_i \in [\omega_1, \omega_2], \quad i = 1, 2, \quad L_1, \ldots, L_{N_1 - 1} \\ \pm j\Delta_2, & \omega_i \in [\omega_3, \omega_4], \quad i = 3, 4, \quad H_1, \ldots, H_{N_2 - 1} \end{cases} \tag{15}$$

where ω_i is the band edge or the in-band frequency point at which $|T(j\omega_i)|$ reaches a local maximum, Δ_1 and Δ_2 are maximum absolute values in the low and high passbands, respectively. Since $N_1 + N_2 = N + 2$, where '2' are contributed by the shunt capacitors at the I/O ports, the number of coefficients to be determined in $T(s)$ is one less than that of constraints after all finite TZs are prescribed. By setting the ripple level in one passband (Δ_1 or Δ_2) as an unknown, an over-determined problem can be avoided. Consequently, the return loss in one of the passbands cannot be arbitrarily prescribed. Using the iterative algorithm proposed in

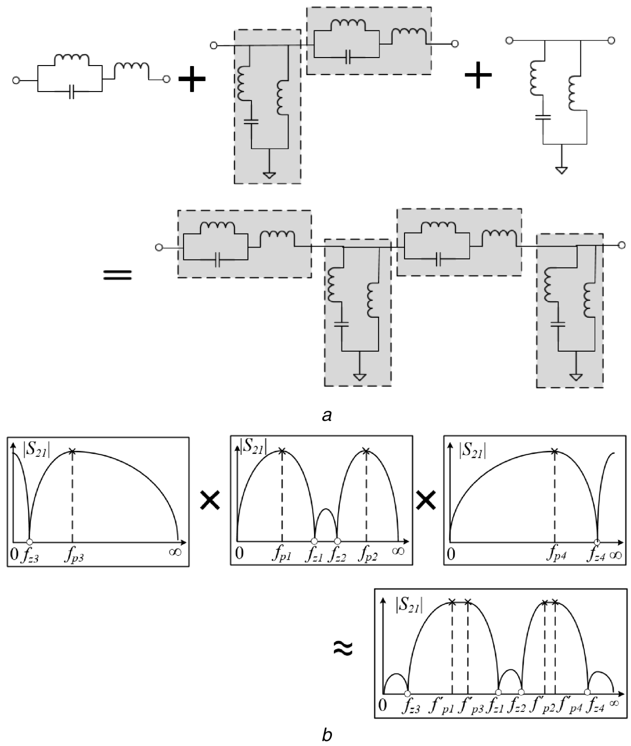

Fig. 6 *Advanced dual-band filter prototype*
(a) Circuit configuration as a cascade of basic dual-band filter and composite series and shunt resonators, ***(b)*** Formation of transmission response by multiplication of individual responses of building blocks

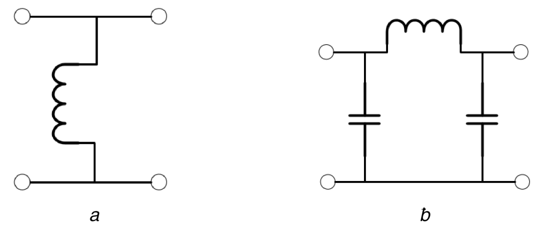

Fig. 7 *Circuit configurations equivalent to the original lumped element circuit at extreme frequencies*
(a) Equivalent circuit at DC, ***(b)*** Equivalent circuit at infinity frequency

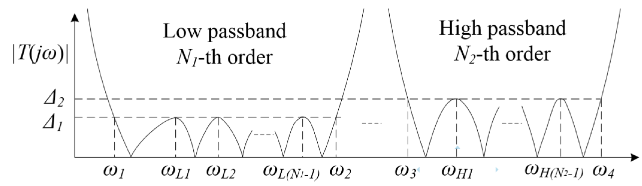

Fig. 8 *Ideal magnitude response of the filtering function*

[21], all the unknowns can be found in several iterations. It is worth mentioning that the return loss in the unspecified passband can be adjusted by changing the locations of finite TZs.

From the filtering function obtained from specifications, the polynomials $E(s)$, $F(s)$, and $P(s)$ can be derived, and then the overall $ABCD$ matrix of the filter prototype can be constructed using the standard transformation. Since each composite series or shunt resonator produces a TZ, it is necessary to appropriately arrange the TZs assigned to each building block in the circuit from the input port (left) to the output port (right) before extraction. With the TZs assigned beforehand, circuit elements can be successively extracted from the $ABCD$ matrix.

The circuit extraction of the proposed filter was not discussed in [17] and is to be elaborated here. Fig. 9 illustrates four basic required circuit extraction operations: extracting a shunt capacitor (Fig. 9*a*); extracting a series inductor and a parallel connected LC series circuit (Fig. 9*b*); extracting a shunt inductor and a serially connected LC tank (Fig. 9*c*); and extracting the remainder circuit consisting of two shunt inductors and a series inductor (Fig. 9*d*). In Fig. 9*a*, the shunt capacitor does not introduce a TZ at either DC or any finite frequency. In other words, extraction of the shunt capacitor does not change the roots of the denominator polynomial. Therefore

$$P_1 = P_r. \tag{16}$$

In Figs. 9*b* and *c*, the L_{ri} and C_{ri} resonator circuit to be extracted produces a TZ at s_{zi}. Consequently, extraction of such a circuit will lead to the denominator polynomial excluding the roots of $\pm s_{zi}$. Therefore, the denominator polynomials P_1 and P_r are related by

$$P_1 = \left(s^2 - s_{zi}^2\right)P_r. \tag{17}$$

To extract the shunt capacitor in Fig. 9*a*, one can terminate the output port with a short circuit. Then the input admittance Y_{in} will be dominated by the shunt capacitor when the frequency tends to infinity. In other words

$$Y_{in} = \frac{D_{1n}}{B_{1n}} = sC_{pi} \quad \text{if } s \to j\infty. \tag{18}$$

Therefore, the shunt capacitance can be extracted as

$$C_{pi} = \left.\frac{D_{1n}}{sB_{1n}}\right|_{s=j\infty} \tag{19}$$

The remainder $ABCD$ matrix can be then obtained with C_{pi} known and prepared for extraction of other circuit elements.

The circuit extraction operations in Figs. 9*b* and *c* have been discussed in [16] and are not restated here. In Fig. 9*d*, the element values can be extracted as

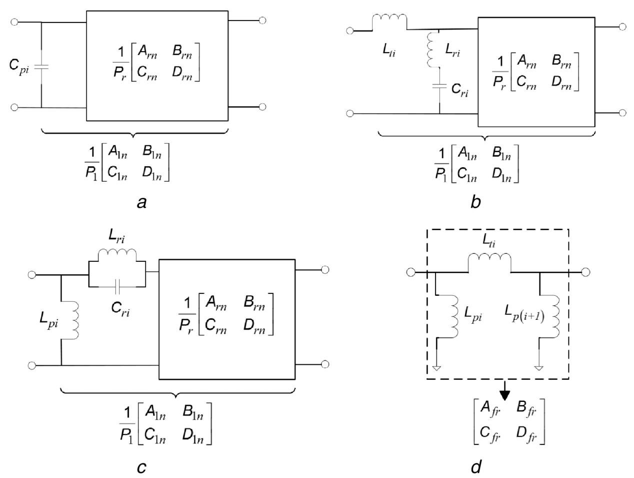

Fig. 9 *Four basic circuit extraction operations*
(a) Extraction of a shunt capacitor, ***(b)*** Extraction of a series inductor and a parallel connected LC series circuit, ***(c)*** Extraction of a shunt inductor and a serially connected LC tank, ***(d)*** Extraction of a Π network of inductors

$$L_{ti} = \frac{B_{fr}}{s}, \quad L_{p1} = \frac{B_{fr}}{\left(D_{fr} - 1\right)s}, \quad L_{p2} = \frac{B_{fr}}{\left(A_{fr} - 1\right)s} \tag{20}$$

The entire extraction procedure may be somewhat different for different arrangement of composite series and shunt resonators. For illustration, the dual-band filter designed in [17] is used here to show the sequential extraction procedure. Fig. 10 shows the circuit prototype of the dual-band filter comprising four shunt resonators and three series resonators. The whole circuit has been divided into ten basic blocks to be extracted in the sequence labelled as extraction step in Fig. 10. The extraction is carried out alternatively from port 1 and port 2. Since the port 1 is treated as the input port in the discussion, the terms '*A*' and '*D*' in the *ABCD* matrix have to be exchanged when using given formulas if the extraction is carried out at port 2. The extraction procedure can be summarised as:

i. Extracting C_{p1} from port 1;
ii. Extracting C_{p2} from port 2;
iii. Extracting L_{t1}, L_{r1}, and C_{r1} from port 1;
iv. Extracting L_{t8}, L_{r7}, and C_{r7} from port 2;
v. Extracting L_{p1}, L_{r2}, and C_{r2} from port 1;
vi. Extracting L_{p7}, L_{r6}, and C_{r6} from port 2;
vii. Extracting L_{t2}, L_{r3}, and C_{r3} from port 1;
viii. Extracting L_{t6}, L_{r5}, and C_{r5} from port 2;
ix. Extracting L_{p3}, L_{r4}, and C_{r4} from port 1;
x. Finally, the extraction procedure ends up at extracting L_{t4}, L_{p4}, and L_{p5}.

Note that, the extracted shunt inductance L_{p4} in the final step is infinity because the filter circuit is strictly symmetrical.

To ensure all the extracted element values are realisable, one must carefully choose the number of composite series and shunt resonators according to the number of TPs in the two passbands and TZs in the stopbands. Fig. 11 shows a typical transmission response of the dual-wideband filter and the attribution of TZs to resonators depending on which passband the two extra TPs are assigned to. For the dual-band filter designed in [17], the two extra TPs are placed in the high passband. Basically, the attribution of TZs should follow the principle of the relative positions of TP and TZ for the composite series and shunt resonators. For instance, the TZs in the low stopband must be produced by composite series resonators as they are below their associated TPs. As shown in Fig. 11*b*, the n_{z1} TZs in the low stopband are produced by n_{z1} composite series resonators, which produce n_{z1} TPs in the low passband; the remaining $N_1 - n_{z1}$ TPs in the low passband are produced by $N_1 - n_{z1}$ composite shunt resonators. By the same token, in the high passband, n_{z3} TPs accompanied by n_{z3} TZs in the upper stopband are produced by n_{z3} composite shunt resonators; two extra TPs are attributed to the two shunt capacitors at the I/O ports; the other $N_2 - n_{z3} - 2$ TPs are all produced by the composite series resonators. Therefore, the total number of composite series and shunt resonators are $N_2 + n_{z1} - n_{z3} - 2$ and $N_1 + n_{z3} - n_{z1}$, respectively. Similarly, according to Fig. 11*a*, there are $N_2 + n_{z1} - n_{z3}$ composite series resonators and $N_1 + n_{z3} - n_{z1} - 2$ composite shunt resonators for the case that the two extra TPs are

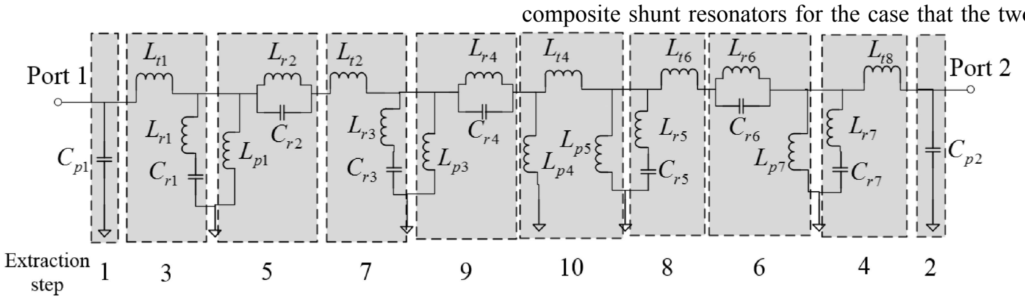

Fig. 10 *Dual-band filter in [17] that comprises four composite shunt resonators and three composite series resonators*

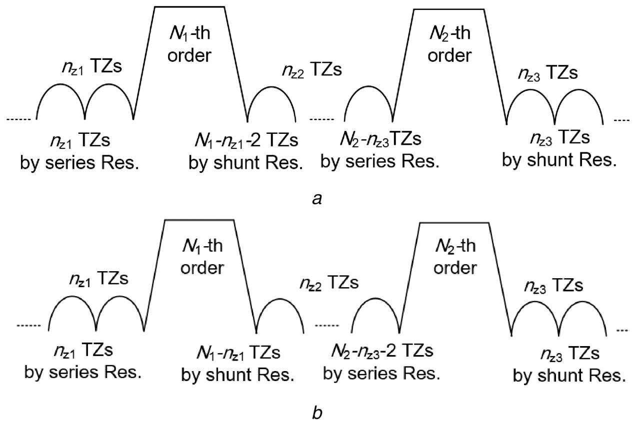

Fig. 11 *Typical responses of the proposed dual-band filter and the attribution of TZs to composite series and shunt resonators in two cases*
(a) Two extra TPs are located in the low passband, ***(b)*** Two extra TPs are located in the high passband

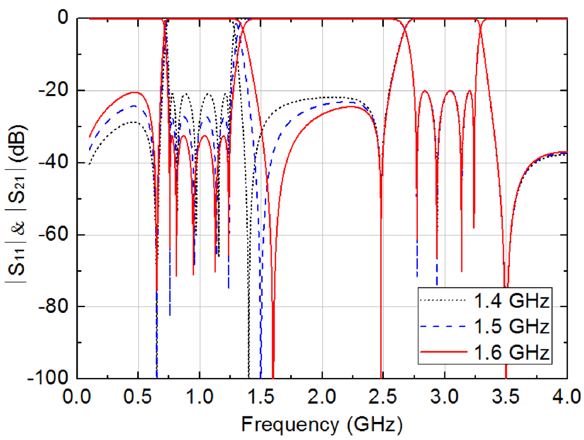

Fig. 12 *Synthesised responses for the double TZ around the upper band edge of the low passband being located at 1.4, 1.5, and 1.6 GHz*

located in the low passband. After the number of composite series and shunt resonators being determined, a trade-off needs to be made between the flexibility of prescribing TZs and the realisability of the corresponding circuit.

Generally, the design option with the two extra TPs being located in the low passband is suitable for the application where the ratio of FBW of the high passband to the low passband is small. On the contrary, if the ratio of FBW is relatively large, it is more appropriate to place the two extra TPs in the high passband.

5 Design examples

Different from the dual-wideband filter in [17], the two extra TPs are placed in the low passband in the two design examples in this paper. The first example filter that is with $N_1 = 5$ and $N_2 = 4$ has a large centre frequency ratio of 3:1. Two far TZs are introduced to suppress the spurious resonances by making use of the parasitic resonance of radial stubs. To make the circuit model in good accordance with realisation, the parasitic inductance of a radial stub should be small enough and thus the generated far TZ is suitable for suppression of spurious resonances that are far away from the high passband. The second example filter is with $N_1 = 5$ and $N_2 = 6$ and the centre frequency ratio of 2:1. Two band-stop blocks of shunt connected series *LC* circuits are inserted in the filter prototype for producing controllable far TZs to suppress the spurious resonances nearest to the high passband. Note that, the inserted bandstop circuits not only produce far TZs but also contribute TPs within the passbands. To ensure the synthesised circuit model realisable, the far TZs should not be too far away from the high passband. For the two example filters, the leading composite resonators from each I/O port are of series type instead of shunt type as those in Fig. 10. As a result, the extraction procedures are slightly different from that discussed in the previous section.

Table 1 Roots of $F(s)$ in each iteration for Example 1

Roots of $F(s)$	1st	2nd	3rd	4th
$\pm s_1$	±j0.751	±j0.756	±j0.756	±j0.756
$\pm s_2$	±j0.864	±j0.808	±j0.813	±j0.813
$\pm s_3$	±j0.991	±j0.968	±j0.956	±j0.957
$\pm s_4$	±j1.123	±j1.140	±j1.138	±j1.137
$\pm s_5$	±j1.244	±j1.238	±j1.238	±j1.238
$\pm s_6$	±j2.766	±j2.772	±j2.772	±j2.772
$\pm s_7$	±j2.929	±j2.934	±j2.936	±j2.936
$\pm s_8$	±j3.095	±j3.139	±j3.137	±j3.137
$\pm s_9$	±j3.245	±j3.238	±j3.238	±j3.238

5.1 Dual-wideband filter with far TZs by radial stubs

The low and high passband of the filter are centred at 1 GHz with $\text{FBW}_1 = 50\%$ and 3 GHz with $\text{FBW}_2 = 16.7\%$, respectively. There are totally seven flexible TZs, which are arranged at 0.65, 3.5, 1.5, 2.48, 1.5, 3.5, 0.65 GHz assigned to the building blocks from the left to right one by one. As has been discussed previously, the filtering function can be determined through the iterative procedure. For illustration, the reflection zero frequencies that have been normalised by $2\pi \times 10^9$ in each iteration are summarised in Table 1. As can be observed, the roots of $F(s)$ converge after four iterations. Generally, the converged solution exhibits different return loss levels in the two passbands. However, the difference can be minimised by adjusting TZs. For instance, the double TZ around the upper band edge of the low passband is set to 1.4, 1.5, or 1.6 GHz, and their corresponding synthesised responses are shown in Fig. 12 for comparison. As can be seen, the difference between the return loss levels in two passbands becomes smaller as the double TZ approaches the band edge. The same result can be also achieved by adjusting other TZs. Generally, the passband would have a higher return loss for a steeper skirt selectivity by moving TZs closer to the passband. Fig. 13 shows the synthesised circuit prototype that consists of four composite series resonators and three composite shunt resonators. Using (1)–(3), the series resonators are all configured in the realistic forms that take into account the parasitic inductance L_i ($i = 1$, 3, 5, and 7) of chip capacitor and its connecting terminals in physical implementation. The parasitic inductance of chip capacitor can be obtained from the circuit model provided by the capacitor manufacturer, whereas the parasitic inductance of connecting terminals can be extracted from EM simulation. Having had the circuit model of filter extracted, the element values can be found and are listed in Table 2. It is worth mentioning that to ensure the shunt inductor L_{p4} is realisable, the TZ produced by the composite shunt resonator that contains L_{p4} may need some adjustment. Here, the TZ produced by series L_{r4} and C_{r4} is set to 2.48 GHz so that the shunt inductor L_{p4} has a quite large inductance. As a result, it can be removed with the filter response affected very little.

To implement the designed filter circuit, all the inductors are realised by HITLs, whereas all the series capacitors in the composite series resonators are implemented by Murata 0402 GJM series chip capacitors. Specifically, C_1 and C_7 are implemented by 7.5 pF chip capacitors, whereas C_3 and C_5 are implemented by 2.4 pF chip capacitors. Radial stubs are used to realise two shunt capacitors at the I/O ports. For the composite shunt resonators, capacitors C_{r2} and C_{r6} are realised by radial stubs but C_{r4} is implemented by a 2 pF chip capacitor for the convenience of layout design. Thanks to the nature of the lumped element circuit, the initial layout for each composite resonator building block can be designed independently, as discussed in Section 2. Due to the existence of parasitic effects, the initial layout dimensions have to be optimised. The final designed layout of the synthesised prototype is shown in Fig. 14. Due to the parasitic inductance, the radial stubs used to realise the shunt capacitors at the I/O ports can

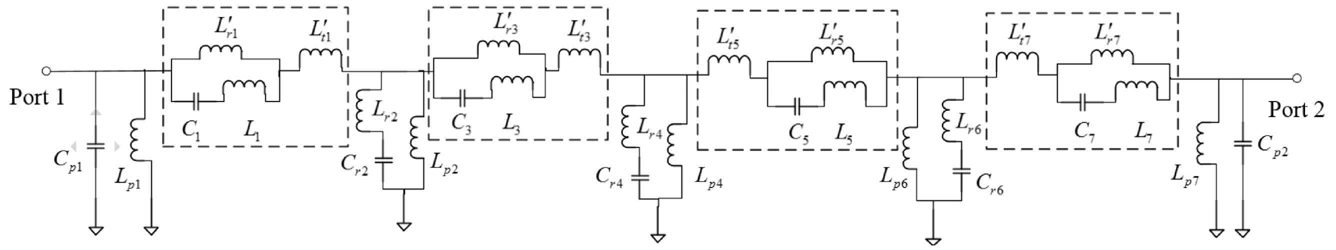

Fig. 13 *Lumped element circuit prototype of the first example filter with all composite series resonators configured in realistic forms that are in accordance with the physical implementation*

Table 2 Circuit element values of filter prototype for Example 1 (inductance in nH, capacitance in pF)

Element indices i	L'_{ti}	L_{pi}	L_{ri} or L'_{ri}	L_i	C_i or C_{ri}	C_{Pi}
1	0.712	10.79	7.172	0.85	7.474	2.698
2	—	9.406	1.432	—	1.444	—
3	0.547	—	3.962	0.77	2.379	—
4	—	338.6	1.965	—	2.096	—
5	0.547	—	3.962	0.77	2.379	—
6	—	9.406	1.432	—	1.444	—
7	0.712	10.79	7.172	0.85	7.474	2.698

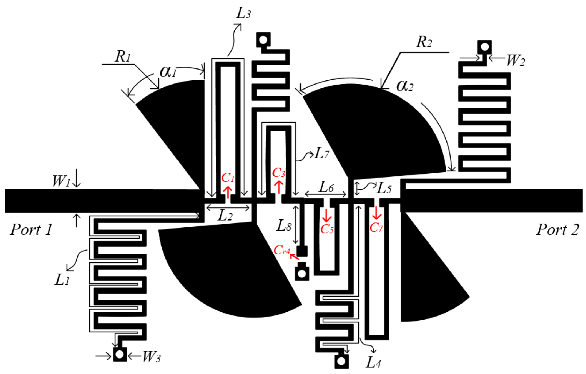

Fig. 14 *Layout of the first example dual-band filter. Dimensions:* $W_1 = 1.40$ *mm,* $W_2 = 0.23$ *mm,* $W_3 = 0.80$ *mm,* $L_1 = 43.20$ *mm,* $L_2 = 3.02$ *mm,* $L_3 = 18.40$ *mm,* $L_4 = 21.29$ *mm,* $L_5 = 1.22$ *mm,* $L_6 = 2.74$ *mm,* $L_7 = 10.44$ *mm,* $L_8 = 2.74$ *mm,* $R_1 = 6.96$ *mm,* $R_2 = 5.90$ *mm,* $\alpha_1 = 37.4°$*,* $\alpha_2 = 114.6°$

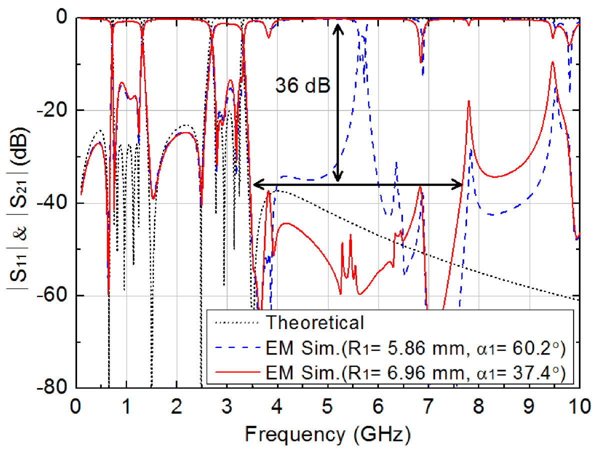

Fig. 15 *Theoretical and EM model simulated responses for two design cases of the radial stubs at I/O ports*

produce TZs that are not expected from the synthesised filter prototype. By properly designing the radius and angle of the radial stub, a desired capacitance and parasitic inductance can be achieved, enabling a low return loss in the passbands and high attenuation at designated frequencies in the upper stopband.

To illustrate the benefit of the far TZs, two sets of dimensions of the radial stubs at the I/O ports are chosen while other dimensions of the filter layout remain the same. In the first case, the radial stub has a radius $R_1 = 5.86$ mm and an angle $\alpha_1 = 60.2°$, which creates a far TZ around 6.5 GHz. In the second case, the radial stub has a radius $R_1 = 6.96$ mm and an angle $\alpha_1 = 37.4°$, which creates a far TZ around 5.3 GHz. The EM simulated filter responses corresponding to the two cases and the theoretical response are superimposed in Fig. 15. As can be observed from the EM simulated response of the first design case, spurious resonances caused by the first and the last series resonator exist around 5.7 GHz. With the radial stub in the second design case, the spurious resonances are effectively suppressed, resulting in an extended upper stopband up to 7.6 GHz (7.6 times the centre frequency of the low passband) with a rejection level of 36 dB. It can be noticed that the EM responses in the passbands in the two cases are almost the same, demonstrating the flexible design of the far TZs. According to the EM simulation, the filter with an extended stopband exhibits an insertion loss of 0.68 and 1.22 dB at the centre frequency of the low and high passbands, respectively. The overall layout has a compact size of $0.12\,\lambda_g \times 0.09\,\lambda_g$, where λ_g is the guided wavelength at the centre frequency of the low passband.

It is noteworthy that the simulated responses in Fig. 15 do not have obvious TPs in the first passband. In the design example in [17] and the second example in this work, one could also find a passband where the simulation does not have obvious TPs. As a common feature, these passbands have a very low theoretical return loss and are susceptible to imperfections such as conductor loss and parasitic couplings between adjacent resonators. It is therefore anticipated that, in these passbands, the simulated responses may deviate obviously from the theoretical ones that having distinct TPs.

5.2 Dual-wideband filter with far TZs by bandstop circuits

The second example filter has its low and high passband centred at 1 GHz with $FBW_1 = 40\%$ and 2 GHz with $FBW_2 = 20\%$, respectively. There are nine flexible TZs prescribed at 0.65, 3.2, 2.4, 1.4, 1.59, 1.4, 2.4, 3.2, 0.65 GHz, corresponding to the composite resonators counting from the left to the right of the circuit shown in Fig. 16, respectively. The two inserted bandstop circuits are shunt connected series LC circuits and can be treated as composite shunt resonators with infinitely large shunt inductances. The bandstop circuits not only produce a double far TZ at 3.2 GHz for suppression of spurious resonances that are caused by the first and last series resonators, but also contribute two TPs in conjunction with the neighbouring connecting inductors. The synthesised circuit element values are given in Table 3. The shunt inductor L_{p5} has a quite large inductance and thus is removed

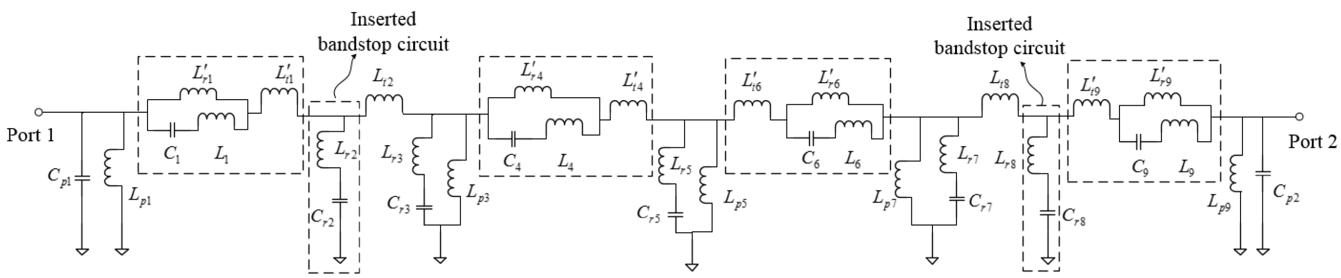

Fig. 16 *Lumped element circuit prototype of the second example filter with two inserted bandstop circuits for generating far TZs*

Table 3 Circuit element values of filter prototype for Example 2 (inductance in nH, capacitance in pF)

Element indices i	L_{ti} or L'_{ti}	L_{pi}	L_{ri} or L'_{ri}	L_i	C_i or C_{ri}	C_{Pi}
1	2.749	6.442	11.31	1.35	4.736	3.009
2	1.146	—	0.555	—	4.460	—
3	—	2.461	1.200	—	3.666	—
4	0.597	—	1.517	0.66	5.936	—
5	—	95.83	2.768	—	3.620	—
6	0.597	—	1.517	0.66	5.936	—
7	—	2.461	1.200	—	3.666	—
8	1.146	—	0.555	—	4.460	—
9	2.749	6.442	11.31	1.35	4.736	3.009

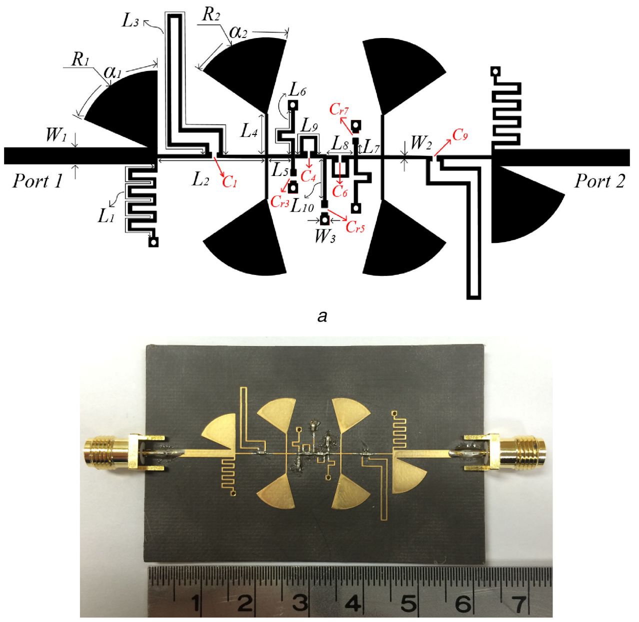

Fig. 17 *Fabricated prototype of the second example dual-band filter*
(a) Layout with dimensional parameters labelled, ***(b)*** Photograph of fabricated prototype dual-band filter
Dimensions: $W_1 = 1.40$ mm, $W_2 = 0.23$ mm, $W_3 = 0.80$ mm, $L_1 = 23.70$ mm, $L_2 = 9.36$ mm, $L_3 = 32.40$ mm, $L_4 = 3.54$ mm, $L_5 = 2.09$ mm, $L_6 = 6.29$ mm, $L_7 = 1.00$ mm, $L_8 = 2.52$ mm, $L_9 = 4.76$ mm, $L_{10} = 3.77$ mm, $R_1 = 6.90$ mm, $R_2 = 6.73$ mm, $\alpha_1 = 66.5°$, $\alpha_2 = 70.2°$

without affecting the response. The substrate used and the way to design the layout dimensions are the same as those used in first design example. The layout and the fabricated prototype are shown in Fig. 17. The capacitors C_1 and C_9 are realised by 4.7 pF chip capacitors, whereas C_4 and C_6 are realised by 6 pF chip capacitors. The two inserted bandstop circuits are realised by a pair of radial-stub-loaded HITLs. Since the capacitors C_{r3}, C_{r5} and C_{r7} in the composite shunt resonators have large capacitances, they are implemented by 3.8 pF chip capacitors instead of radial stubs for the convenience of layout design. The overall layout size is $0.19\lambda_g \times 0.11\lambda_g$.

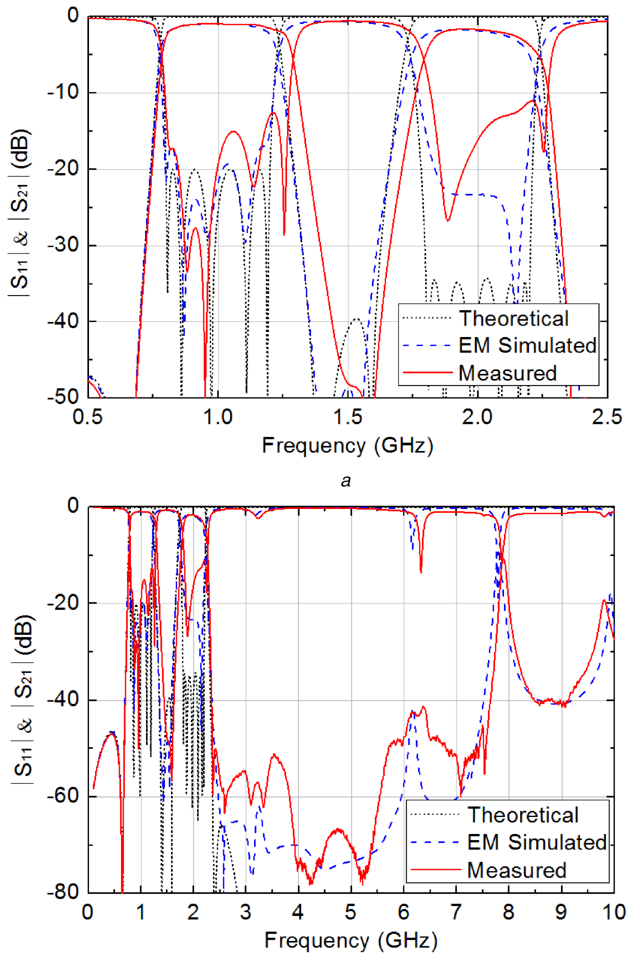

Fig. 18 *Theoretical circuit model, EM simulated, and measured responses of the second example dual-band filter*
(a) Responses within the low and high passbands, ***(b)*** Responses in a broad frequency range

Fig. 18 shows the comparison of the theoretical circuit model, the EM simulated and the measured responses of the second example filter. Good agreement among them is observed even

Table 4 Dual-band filter comparison

Reference	Centre frequencies, GHz	FBW 1/2, %	Order	Size (λ_g^2)	Stopband limit	Resonator type
[4]	3.98/7.94	47.6/48.4	9/9	0.4375	3.2 f_1 (20 dB)	SIR
[9]	0.58/1.41	34.1/12.5	2/2	0.0078	3.3 f_1 (15 dB)	SIR
[10]	0.66/1.34	28.2/18.2	3/3	0.0656	3 f_1 (20 dB)	SIR
[11]	1.2/2.4	10/8	2/2	0.0044	8 f_1 (20 dB)	SIR
[12]	1/2	5/4.1	4/4	0.025	7.1 f_1 (20 dB)	stub-loaded SIR
[13]	2.4/6	5/4.7	4/4	N/A	8.3 f_1 (30 dB)	SIR
[17]	1/2	40/20	4/5	0.012	5 f_1 (30 dB)	quasi-lumped composite resonator
this work 1	1/3	50/16.7	5/4	0.0108	7.6 f_1 (36 dB)	quasi-lumped composite resonator
this work 2	1/2	40/20	5/6	0.0209	7.6 f_1 (40 dB)	quasi-lumped composite resonator

f_1 is the centre frequency of the low passband; λ_g is the guided wavelength at f_1.

though the double TZ prescribed at 1.4 GHz is shifted to a higher frequency, resulting in a slight bandwidth extension of the low passband as can be seen in Fig. 18*a*. The discrepancy is attributed to the fact that the composite series resonators that are responsible for the double TZ have small inductances and thus are realised with small footprints that are sensitive to the fabrication error and hand soldering. To reduce the sensitivity, longer HITLs can be used by choosing a lower characteristic impedance of transmission line. The measured insertion loss at 1 and 2 GHz are 0.92 and 1.67 dB, respectively, which are in good accordance with the EM simulated results of 0.94 dB at 1 GHz, and 1.82 dB at 2 GHz. As can be observed from the measured response in Fig. 18*b*, the filter exhibits a wide spurious-free upper stopband up to 7.6 GHz (7.6 times the centre frequency of the low passband) with a high rejection level of 40 dB.

Regarding the spurious performance, the relative bandwidth of upper stopband achieved here is comparable to that in [16]. The comparison between this work and other references on dual-band filters is shown in Table 4. As can be seen, the upper stopband performance of the two designed filters is obviously better than that in [17] after using the proposed methods of spurious suppression. Compared with other dual-wideband filters in [4, 9, 10], this proposed filter has a remarkable wide upper stopband and compact circuit size. It should take into consideration the filter order when comparing circuit sizes of different designs. Therefore, the compactness of the two filters is comparable to that in [9]. Although the filters in [11–13] have a wide upper stopband, their passbands have limited bandwidths.

Note that, the presented filter design examples in this work and that in [17] have different orders and *FBW*s for the low and high passband. Nevertheless, the proposed filter and its synthesis theory are general and are capable of identical orders and *FBW*s for the two passbands.

6 Conclusion

A novel dual-wideband BPF configuration comprising composite series and shunt resonators is presented in conjunction with its direct synthesis and design theory. The order for each passband can be user defined and multiple TZs can be flexibly assigned on both sides of the low and high passbands to enhance the skirt selectivity and inter-band isolation. To achieve the same return loss in two passbands and to ensure the synthesised circuit realisable, TZs may need some adjustments. A noticeable advantage of the new dual-wideband filter configuration is its wide upper stopband. Specifically, far TZs can be designated at desired frequencies by either adjusting the parasitic inductances of radial stubs at the I/O ports or inserting bandstop blocks of shunt connected series *LC* circuits. Two design examples demonstrate the excellent upper stopband performance of the new filter configuration. Moreover, the proposed filter has a good compact size feature.

7 References

[1] Oshima, S., Wada, K., Murata, R., *et al.*: 'Multilayer dual-band bandpass filter in low-temperature co-fired ceramic substrate for ultra-wideband applications', *IEEE Trans. Microw. Theory Tech.*, 2010, **58**, (3), pp. 614–623

[2] Tsai, L.-C., Hsue, C.-W.: 'Dual-band bandpass filters using equal-length coupled-serial-shunted lines and Z-transform technique', *IEEE Trans. Microw. Theory Tech.*, 2004, **52**, (4), pp. 1111–1117

[3] Sun, S., Zhu, L.: 'Compact dual-band microstrip bandpass filter without external feeds', *IEEE Microw. Wirel. Compon. Lett.*, 2005, **15**, (10), pp. 644–646

[4] Liu, A.-S., Huang, T.-Y., Wu, R.-B.: 'A dual wideband filter design using frequency mapping and stepped-impedance resonators', *IEEE Trans. Microw. Theory Tech.*, 2008, **56**, (12), pp. 2921–2929

[5] Li, Y.C., Wong, H., Xue, Q.: 'Dual-mode dual-band filter based on a stub-loaded patch resonator', *IEEE Microw. Wirel. Compon. Lett.*, 2011, **21**, (10), pp. 525–527

[6] Macchiarella, G., Tamiazzo, S.: 'Design techniques for dual-passband filters', *IEEE Trans. Microw. Theory Tech.*, 2005, **53**, (11), pp. 3265–3271

[7] Bila, S., Cameron, R., Lenoir, P., *et al.*: 'Chebyshev synthesis for multi-band microwave filters'. Proc. IEEE MTT-S Int. Microwave Symp. Digest, San Francisco, CA, June 2006, pp. 1221–1224

[8] Zhang, R., Zhu, L.: 'Synthesis and design of wideband dual-band bandpass filters with controllable in-band ripple factor and dual-band isolation', *IEEE Trans. Microw. Theory Tech.*, 2013, **61**, (5), pp. 1820–1828

[9] Zhang, R., Zhu, L.: 'Synthesis of dual-wideband bandpass filters with source-load coupling network', *IEEE Trans. Microw. Theory Tech.*, 2014, **62**, (3), pp. 441–449

[10] Zhang, R., Luo, S., Zhu, L.: 'Synthesis and design of asymmetrical dual-band bandpass filters with modified richard's transformation', *IET Microw. Antennas Propag.*, 2016, **10**, (12), pp. 1352–1362

[11] Cervera, F.J., Hong, J.: 'Compact self-packaged dual-band filter using multilayer liquid crystal polymer technology', *IEEE Trans. Microw. Theory Tech.*, 2014, **62**, (11), pp. 2618–2625

[12] Wu, S.-R., Hsu, K.-W., Tu, W.-H.: 'Compact wide-stopband microstrip bandpass filter based on stub-loaded stepped-impedance resonators', *IET Microw. Antennas Propag.*, 2012, **6**, (13), pp. 1422–1428

[13] Kuo, J.-T., Lin, H.-P.: 'Dual-band bandpass filter with improved performance in extended upper rejection band', *IEEE Trans. Microw. Theory Tech.*, 2009, **57**, (4), pp. 824–829

[14] Weng, S.-C., Hsu, K.-W., Tu, W.-H.: 'Compact and switchable dualband bandpass filter with high selectivity and wide stopband', *Electron. Lett.*, 2013, **49**, (20), pp. 1275–1277

[15] Li, Z., Wu, K.-L.: 'Direct synthesis and design of a general sequentially coupled wideband bandpass filter with *N*-transmission zeros', *IEEE Trans. Microw. Theory Tech.*, 2016, **64**, (5), pp. 1484–1495

[16] Li, Z., Wu, K.-L.: 'Direct synthesis and design of wideband bandpass filter with composite series and shunt resonators', *IEEE Trans. Microw. Theory Tech.*, 2017, **65**, (10), pp. 3789–3800

[17] Li, Z., Wu, K.-L.: 'Synthesis and design of dual-wideband filter with composite series and shunt resonators'. Proc. IEEE MTT-S Int. Microwave Symp. Digest, Honolulu, HI, June 2017, pp. 360–363

[18] Hong, J.-S., Lancaster, M.J.: '*Microstrip filters for RF/microwave applications*' (John Wiley & Sons, Inc., New York, NY, USA, 2004)

[19] Giannini, F., Paoloni, C., Ruggieri, M.: 'CAD-oriented lossy models for radial stubs', *IEEE Trans. Microw. Theory Tech.*, 1988, **36**, (2), pp. 305–313

[20] Saal, R., Ulbrich, E.: 'On the design of filters by synthesis', *IRE Trans. Circuit Theory*, 1958, **5**, (4), pp. 284–327

[21] Macchiarella, G.: ''Equi-ripple' synthesis of multiband prototype filters using a remez-like algorithm', *IEEE Microw. Wirel. Compon. Lett.*, 2013, **23**, (5), pp. 231–233